clean technologies

MDPI

Article

Defect Properties of $Li_2NiGe_3O_8$

Navaratnarajah Kuganathan [1,*], Raveena Sukumar [2] and Poobalasuntharam Iyngaran [2]

[1] Department of Materials, Faculty of Engineering, Imperial College London, London SW7 2AZ, UK
[2] Department of Chemistry, University of Jaffna, Sir. Pon Ramanathan Road, Thirunelvely, Jaffna 40000, Sri Lanka; raveena@univ.jfn.ac.lk (R.S.); piyngs7@gmail.com (P.I.)
* Correspondence: n.kuganathan@imperial.ac.uk

Abstract: There is a growing interest in finding a suitable electrolyte material for the construction of rechargeable Li-ion batteries. $Li_2NiGe_3O_8$ is a material of interest with modest Li-ionic conductivity. The atomistic simulation technique was applied to understand the defect processes and Li-ion diffusion pathways, together with the activation energies and promising dopants on the Li, Ni, and Ge sites. The Li-Ni anti-site defect cluster was found to be the dominant defect in this material, showing the presence of cation mixing, which can influence the properties of this material. Li-ion diffusion pathways were constructed, and it was found that the activation energy for a three-dimensional Li-ion migration pathway is 0.57 eV, which is in good agreement with the values reported in the experiment. The low activation energy indicated that Li-ion conductivity in $Li_2NiGe_3O_8$ is fast. The isovalent doping of Na, Fe and Si on the Li, Ni and Ge sites is energetically favorable. Both Al and Ga are candidate dopants for the formation of Li-interstitials and oxygen vacancies on the Ge site. While Li-interstitials can improve the capacity of batteries, oxygen vacancies can promote Li-ion diffusion.

Keywords: $Li_2NiGe_3O_8$; Li-ion diffusion; defects; dopants; classical simulation

Citation: Kuganathan, N.; Sukumar, R.; Iyngaran, P. Defect Properties of $Li_2NiGe_3O_8$. *Clean Technol.* **2022**, *4*, 619–628. https://doi.org/10.3390/cleantechnol4030038

Academic Editor: Masoud Baghernejad

Received: 13 March 2022
Accepted: 23 June 2022
Published: 1 July 2022

1. Introduction

The generation of renewable energy is one of the important challenges and requires the development devices such as Li-ion batteries [1–5], Li-ion capacitors [6], novel Na-ion batteries [7], Na-ion capacitors [8] and K-ion batteries [9]. Lithium-ion batteries (LIBs), being one of the very successful types of rechargeable battery for portable electronics, are well known in consumer electronics and have secured a significant role as one of the promising clean energy devices superseding non-renewable fossil fuels. Its outstanding properties generally emanate from its electrode and electrolyte materials. Consequently, scientists are paying attention to the development of new electrode and electrolyte materials with unique electrochemical performance, and environmentally sound and prolific constituent elements.

Recent research studies have focused on investigating novel Lithium-ion conducting electrode and electrolyte materials to be used in rechargeable LIBS. Solid electrolytes are more preferred than liquid electrolytes for portable applications due to the electrochemical instability arising from contact between liquid electrolytes and cathodes [10,11]. Furthermore, solid electrolytes offer a wide range of advantages, e.g., simpler and safer cell design, better shock resistance and durability [12]. To date, research has been done incessantly to develop and optimize suitable candidate materials with Li-ion conductivities of at least 10^{-3} S/cm at ambient temperature [10–12]. Thus, new materials with higher ionic conductivity may be great beneficial for improving the performance of LIBs.

Although most of the solid electrolyte materials have been studied, their applications in commercial cells are limited due to their high interfacial resistance with electrode materials [13,14]. Lowering the interfacial resistance may be the key to the development of a solid electrolyte material.

The spinel structure, with the general formula of AB_2O_4, exhibits a wide range of electrical properties, being a cubic close-packed oxide with eight tetrahedral and four

octahedral sites per formula unit. The arrangement of cations in the spinel structure decides whether the structure is normal ($[A]_{tet}[B_2]_{oct}O_4$), inverse ($[B]_{tet}[A,B]_{oct}O_4$) or random ($[B_{0.67}A_{0.33}]_{tet}[A_{0.67}B_{1.33}]_{oct}O_4$) [15,16]. Li-based spinels have been studied to investigate their fascinating electrical properties, as they follow a two-step conduction mechanism with the formation of a three-dimensional 8a-16c-8a pathway [17].

$Li_2NiGe_3O_8$ is an ordered or 'complex' spinel structure that can serve as a potential candidate material, since it does not exhibit any phase transitions upon heating or any cation mixing across tetrahedral or octahedral sites [10,11]. $Li_2NiGe_3O_8$ is a synthetic material belonging to the space group of $P4_332$, which exhibits modest Li-ion conductivity of ~10^{-5} S/cm at 63 °C [10]. The conduction of the Li-ion in $Li_2NiGe_3O_8$ occurs via a simple 8c-12d-8c hopping mechanism [10] with an activation energy of 0.43 ± 0.03 eV at 300 K [11]. Therefore, this can be considered as an ideal candidate material for studying its electrical properties further. Though few studies on the diffusion of Li-ions and the electrochemical studies are available, theoretical reports on the intrinsic defects, diffusion pathways and solution of dopants are not available in the literature.

Since defect studies on this material have not been explored yet, we used a computational modelling technique based on the classical pair potentials to investigate defect energetics and diffusion pathways, together with activation energies and promising dopants. Defect calculations can provide useful information about the defect processes (Schottky, Frenkel and anti-site) influencing the electrochemical properties of this material. Through use of the current methodology, long range Li-ion diffusion pathways and their activation energies can be simulated. Such information is crucial for optimizing this solid electrolyte material in all solid-state LIBs. The promising isovalent or aliovalent dopants predicted from this study can be considered for experimental verification.

2. Computational Methods

The bulk and defective structure calculations were based on the Buckingham potentials as implemented in GULP (General Utility Lattice Program) code [18]. In this method, total lattice energy or interactions between ions were modelled using long-range Coulombic interaction and short-range repulsive interactions representing electron–electron repulsion and van der Waals interactions. Buckingham potentials [19–21] were used to model short-range interactions (see Table 1). The potentials used for the dopant oxides are provided in the supplementary information (Table S1). The full structural relaxation of the atom positions and simulation boxes was performed using the Broyden–Fletcher–Goldfarb–Shanno (BFGS) algorithm [22]. The defect process was assumed to take place under constant pressure. Lattice relaxations around point defects and migrating ions were modelled using the Mott–Littleton method [23]. This method partitions a crystal lattice into two spherical regions. Region I contained ions surrounding the defect, which are explicitly relaxed, and Region II was treated by using quasi-continuum methods. The activation energy of the migration is the energy difference between the initial configuration and a saddle point configuration. In all optimized configurations, the forces on the atoms were less than 0.001 eV. The defects' enthalpies will be overestimated, as the present model assumes a full charge ionic model, with the calculation corresponding to the dilute limit. A schematic representation of the defect models is shown in the supplementary information (see Supplementary Figure S1).

Table 1. Buckingham potential parameters [19–21] used in classical simulations of $Li_2NiGe_3O_8$.

Interaction	A/eV	ρ/Å	C/eV•Å^6	Y/e	K/eV•Å^{-2}
$Li^+ - O^{2-}$	632.1018	0.2906	0	1	99,999.0
$Ni^{2+} - O^{2-}$	1760.0	0.2800	0	2	93.7
$Ge^{4+} - O^{2-}$	1497.3996	0.325646	16.808599	4	99,999.0
$O^{2-} - O^{2-}$	22,764.30	0.1490	44.53	−2.96	65.0

3. Results and Discussion

3.1. Modelling of Bulk $Li_2NiGe_3O_8$

The crystal structure of $Li_2NiGe_3O_8$ is cubic with the space group of $P4_332$. The experimentally observed crystal structure has the lattice parameters a = b = c = 8.180 Å and $\alpha = \beta = \gamma = 90^\circ$ [11]. In this complex structure, Li-ions form a tetrahedral coordination (see Figure 1). Both the Ni^{2+} and Ge^{4+} ions are bonded to the nearest neighboring O^{2-} ions, forming distorted octahedral units. The LiO_4 tetrahedral units share their corners with the neighboring NiO_6 and GeO_6 octahedral units. Full geometry optimization was performed to calculate the equilibrium lattice constants. The calculated lattice constants are in good agreement with those reported in the experiment (see Table 2) indicating the suitability of the potential parameters used in this study.

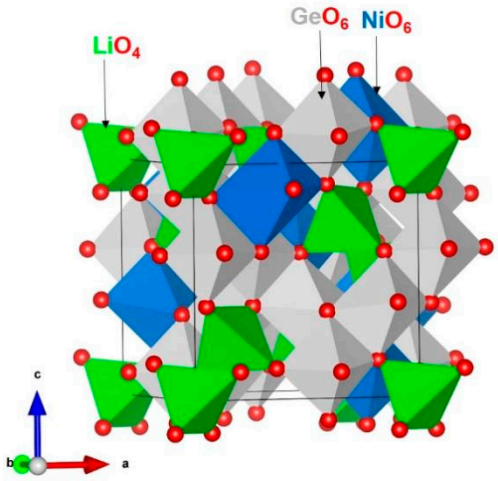

Figure 1. Crystallographic structure of a $Li_2NiGe_3O_8$ spinel.

Table 2. Calculated and experimental lattice parameters of a $Li_2NiGe_3O_8$ spinel.

Parameter	Calculated	Experiment [11]	| Δ | (%)
a = b = c (Å)	8.218	8.180	0.46
$\alpha = \beta = \gamma$ (°)	90	90	0
V (Å^3)	555.11	547.39	1.41

3.2. Intrinsic Defects

In this section, we discuss the formation of possible intrinsic defects in $Li_2NiGe_3O_8$. Isolated point defects (vacancies and interstitials) were first generated, and their formation energies were calculated. Frenkel, Schottky and anti-site defect formation energies were then calculated by associating appropriate point defect energies. The electrochemical and diffusion properties of a material are influenced by these defect processes. Anti-site defects have been found both experimentally and theoretically in many oxides [24–28]. We considered anti-site defects in isolated and cluster form. In the cluster form, isolated defects were considered in the same supercell. In the isolated form, isolated defect energies were calculated separately and their energies were combined. The defect reaction equations were constructed using Kröger–Vink notation [29].

$$\text{Li Frenkel}: \ Li_{Li}^{X} \rightarrow V_{Li}^{\prime} + Li_{i}^{\bullet} \quad (1)$$

$$\text{Ni Frenkel}: \ Ni_{Ni}^{X} \rightarrow V_{Ni}^{\prime\prime} + Ni_{i}^{\bullet\bullet} \quad (2)$$

$$\text{Ge Frenkel}: \ Ge_{Ge}^{X} \rightarrow V_{Ge}^{\prime\prime\prime\prime} + Ge_{i}^{\bullet\bullet\bullet\bullet} \quad (3)$$

$$\text{O Frenkel}: \ O_{O}^{X} \rightarrow V_{O}^{\bullet\bullet} + O_{i}^{\prime\prime} \quad (4)$$

$$\text{Schottky}: \ 2Li_{Li}^{X} + Ni_{Ni}^{x} + 3Ge_{Ge}^{X} + 8O_{O}^{X} \rightarrow \ 2V_{Li}^{\prime} + V_{Ni}^{\prime\prime} + 3V_{Ge}^{\prime\prime\prime\prime} + 8V_{O}^{\bullet\bullet} + \ Li_2NiGe_3O_8 \quad (5)$$

$$Li_2O \text{ Schottky}: \ 2Li_{Li}^{X} + \ O_{O}^{X} \ \rightarrow \ 2V_{Li}^{\prime} + \ V_{O}^{\bullet\bullet} + Li_2O \quad (6)$$

$$NiO \text{ Schottky}: \ Ni_{Ni}^{X} + \ O_{O}^{X} \ \rightarrow \ V_{Ni}^{\prime\prime} + \ V_{O}^{\bullet\bullet} + NiO \quad (7)$$

$$GeO_2 \text{ Schottky}: \ Ge_{Ge}^{X} + 2O_{O}^{X} \ \rightarrow \ V_{Ge}^{\prime\prime\prime\prime} + 2 \ V_{O}^{\bullet\bullet} + GeO_2 \quad (8)$$

$$Li/Ni \text{ antisite (isolated)}: \ Li_{Li}^{X} + \ Ni_{Ni}^{X} \ \rightarrow \ Li_{Ni}^{\prime} + \ Ni_{Li}^{\bullet} \quad (9)$$

$$Li/Ni \text{ antisite (cluster)}: \ Li_{Li}^{X} + \ Ni_{Ni}^{X} \ \rightarrow \ \left\{Li_{Ni}^{\prime} : Ni_{Li}^{\bullet}\right\}^{X} \quad (10)$$

$$Ni/Ge \text{ antisite (isolated)}: \ Ni_{Ni}^{X} + \ Ge_{Ge}^{X} \ \rightarrow \ Ni_{Ge}^{\prime\prime} + \ Ge_{Ni}^{\bullet\bullet} \quad (11)$$

$$Ni/Ge \text{ antisite (cluster)}: \ Ni_{Ni}^{X} + \ Ge_{Ge}^{X} \ \rightarrow \ \left\{Ni_{Ge}^{\prime\prime} : Ge_{Ni}^{\bullet\bullet}\right\}^{X} \quad (12)$$

We report the defect energies calculated for all defect processes in Figure 2. The lowest energy defect is the Li-Ni anti-site defect cluster. This shows that Li/Ni cation disorder will be present although the exact concentration is unknown. The Ni/Ge anti-site defect cluster exhibits slightly greater energy than that calculated for the isolated Li/Ni anti-site. This is because of the charge difference (+2) between Ni^{2+} and Ge^{4+} is greater than that that found (+1) between Li^{+} and Ni^{2+}. The favorability of the anti-site defect cluster is due to the exoergic binding of isolated defects. The Li-Frenkel defect energy is 1.74 eV. This defect process will ensure the formation of Li vacancies and enhance the vacancy-assisted Li-ion migration in this material. The other Frenkel and Schottky energies are highly exothermic and require a high temperature.

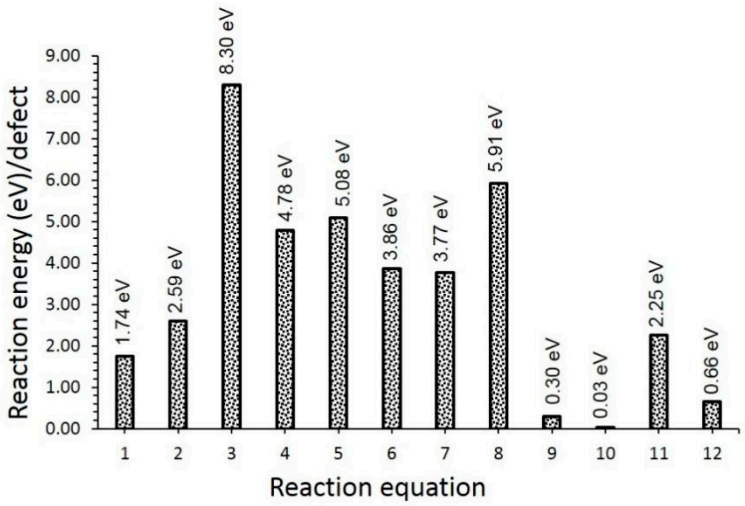

Figure 2. Defect reaction energies for different defect processes.

3.3. Li-ion Diffusion

Materials with fast diffusion of Li-ions and low activation energy can enhance the performance of Li-ion batteries. The current simulation technique was successfully used on various oxide materials to elucidate the diffusion pathways and activation energies [30–33]. Here, we constructed long Li-ion diffusion pathways by considering local Li-Li hops and calculated the activation energies for local hops.

Two promising Li local hops with Li-Li separations of 3.55 Å and 3.58 Å were identified (see Figure 3a). The activation energies for these hops were calculated to be 0.57 eV and 0.89 eV, respectively (see Figure 3b,c). We have considered Li hop distances longer than 4.00 Å. However, their activation energies were prohibitively high, with activation barriers greater than 3.00 eV. Long-range Li-ion migration pathways were identified by connecting local hops. Two promising long-range pathways ((A→A→A→A) and

(A→A→B→A)) were identified. The lowest activation energy (0.57 eV) was noted for the A→A→A→A long-range pathway. Daniel et al. [11] evaluated the Li-ion diffusion mechanism in $Li_2NiGe_3O_8$ and reported that the bulk Li-ion diffusion activation energies of powdered samples and samples sintered at 950 °C are 0.43 ± 0.03 eV and 0.53 ± 0.01 eV, respectively. The values reported in the experimental study agree with the value calculated in this study. Both the experiment and theory concluded that Li-ion diffusion in this material is fast.

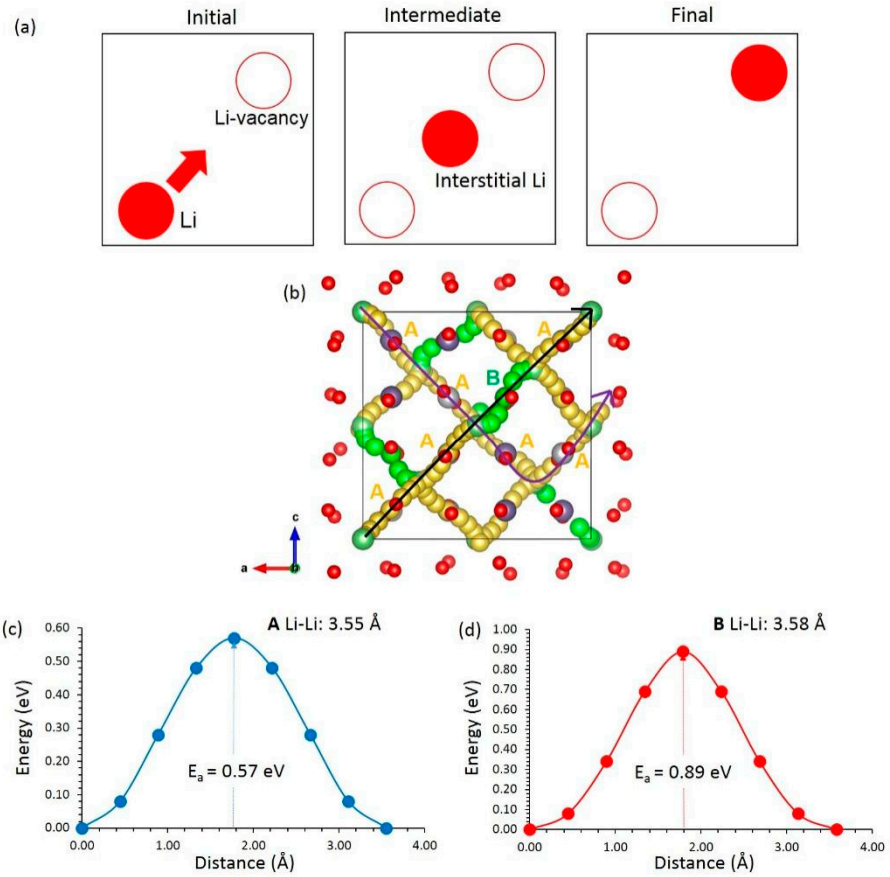

Figure 3. (**a**) Schematic diagram showing the stages of vacancy-mediated Li-ion migration (**b**) Li-ion diffusion pathways and (**c**,**d**) energy profile diagrams showing the activation energies of the local hops A and B, respectively.

3.4. Solution of Dopants

A range of isovalent and aliovalent dopants were substituted on the Li, Ni and Ge sites. The aliovalent doping required charge-compensating defects in the lattice. In all doping processes, the lattice energies of oxides were used to construct the defect reactions. The candidate dopants can be used to modify the mechanical, electronic and chemical properties of $Li_2NiGe_3O_8$.

3.4.1. Alkali Dopants

Three alkali metal ions (Na^+, K^+ and Rb^+) were doped on the Li site. The solution energies were calculated by using the following equation:

$$M_2O + 2Li_{Li}^X \rightarrow 2M_{Li}^X + Li_2O \quad (13)$$

A negative solution energy calculated for Na^+ means this dopant is thermodynamically feasible (see Figure 4). This is partly due to the fact that the ionic radius of Na^+ ions (1.02 Å) is reasonably close to that of Li-ions (0.76 Å). The solution energy increases gradually with

increasing ionic radius. The solution energy is highly endoergic (4.89 eV) for Rb^+, and this dopant is thermodynamically unfavorable. A possible chemical composition that can be synthesized is $Li_{2-x}Na_xNiGe_3O_8$ ($0.0 < x < 1.0$), although the exact concentration can be determined by experiments.

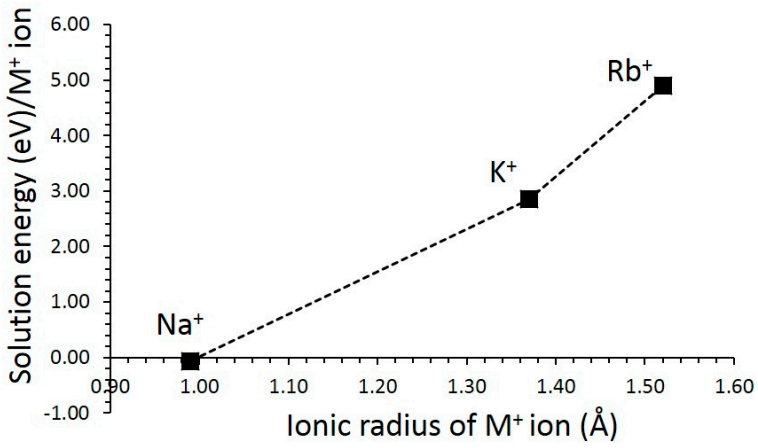

Figure 4. Calculated solution energies of M_2O with respect to the M^+ ionic radius in $Li_2NiGe_3O_8$.

3.4.2. Divalent Dopants

A range of divalent cations consisting of transition metal cations and alkali earth cations were considered on the Ni site. The defect reaction required no charge-compensating defects, as explained by the following equation.

$$MO + Ni_{Ni}^{X} \rightarrow M_{Ni}^{X} + NiO \quad (14)$$

The calculated solution energies show that the most promising dopant is Fe^{2+}, with a solution energy of −1.19 eV (see Figure 5). Very low solution energies were calculated for Co^{2+}, Mn^{2+}, Cu^{2+} and Zn^{2+}. The promising feature of these five dopants is partly due to their ionic radii closely matching with the ionic radius of Ni^{2+} (0.69 Å). The solution energy gradually increases with an increasing ionic radius. The Ba^{2+} has a very large positive solution energy of 4.32 eV, and this dopant is highly unfavorable.

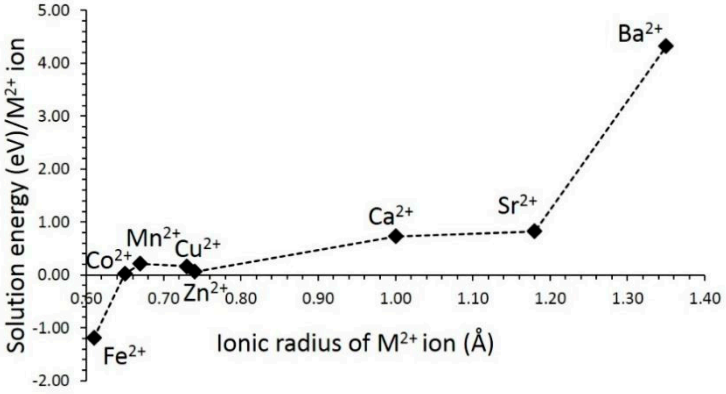

Figure 5. Calculated solution energies of MO with respect to the M^{2+} ionic radius in $Li_2NiGe_3O_8$.

3.4.3. Trivalent Dopants

The substitution of trivalent dopants on the Ge site can create two charge compensating defects, namely lithium interstitials and oxygen vacancies in the lattice. Additional Li-ions

in this material would enhance the capacity of $Li_2NiGe_3O_8$ in the form of Li-interstitials according to Equation (15):

$$M_2O_3 + 2\,Ge_{Ge}^{X} + Li_2O \rightarrow\ 2\,M'_{Ge} + 2\,Li_i^{\bullet} + 2\,GeO_2 \quad (15)$$

The Al^{3+} was found to be the most favorable dopant for this process (see Figure 6). This is due to the fact that the ionic radius of Al^{3+} (0.54 Å) is very close to the ionic radius of Ge^{4+} (0.53 Å). The solution energy of Ga^{3+} is higher than that calculated for Al^{3+} by only 0.07 eV. The solution energy increases with an increasing ionic radius. The most unfavorable dopant for this process is La^{3+}.

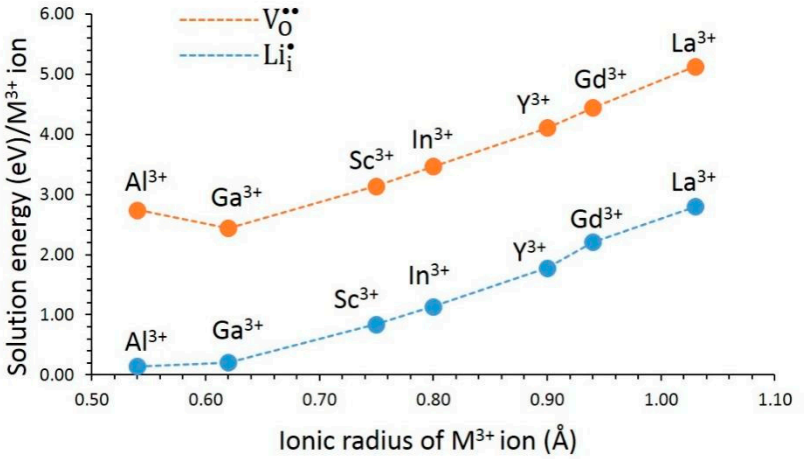

Figure 6. Calculated solution energies of M^{3+} ions on the Ge site. Blue and orange plots correspond to the formation of Li-interstitials and O-vacancies respectively.

Vacancy-assisted Li-ion migration can be promoted by the oxygen vacancies via the formation of Li_2O. As mentioned above, oxygen vacancies require doping of trivalent cations on the Ge site, as explained by the following equation.

$$M_2O_3 + 2\,Ge_{Ge}^{X} + O_O^{X} \rightarrow\ 2\,M'_{Ge} +\ V_O^{\bullet\bullet} + 2\,GeO_2 \quad (16)$$

In general, higher solution energies were noted for this process compared with those calculated for the Li-interstitial charge compensation (see Figure 6), meaning that this process requires high temperatures. Ga^{3+} is a suitable dopant for this process, although the solution energy of Al^{3+} is lower than that calculated for Ga^{3+} by only 0.03 eV. Again, La^{3+} is an unfavorable dopant for this process.

3.4.4. Tetravalent Dopants

The Ge site was replaced by different tetravalent cations (Si^{4+}, Sn^{4+}, Ti^{4+}, Zr^{4+} and Ce^{4+}). The doping of tetravalent cations introduces no charge-compensating defects according to Equation (17):

$$MO_2 +\ Ge_{Ge}^{X}\ \rightarrow M_{Ge}^{X}\ + GeO_2 \quad (17)$$

The most favorable dopant is Si^{4+} (see Figure 7), as it exhibits a negative solution energy of −1.13 eV. Ti^{4+} is the second most favorable dopant. As this dopant has an exoergic solution energy of −0.39 eV, this dopant is also worth testing experimentally. Positive solution energies were noted for other dopants. In particular, the solution energy calculated for Ce^{4+} is 3.07 eV.

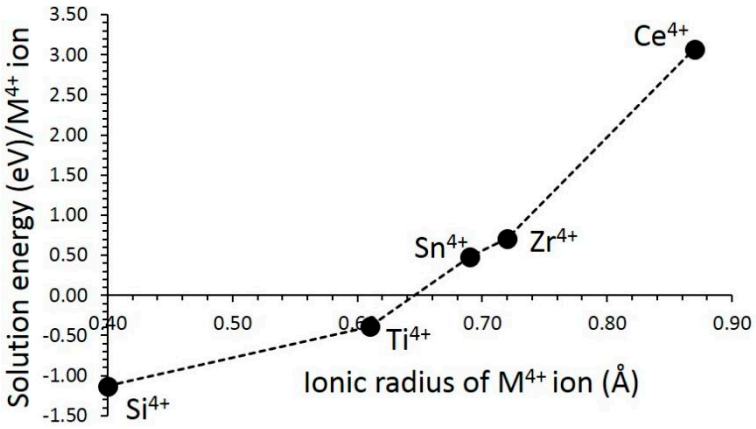

Figure 7. Calculated solution energies of MO_2 with respect to the M^{4+} ionic radius in $Li_2NiGe_3O_8$.

3.5. The Impact of Favorable Dopants on the Diffusion of Li-ions

Li-ion diffusion pathways were calculated in the presence of the most favorable dopants. Table 3 reports the activation energies. Doping with Na increased the activation energies of local Li hops A and B slightly. There was a small reduction in the activation energies upon Fe doping. Both Al and Ga also exhibited a very small decrease in the activation energies. Doping with Si on the Ge site had almost no effect on the activation energies. In the current study, the dopant concentration was 1.8%. Further increases in the dopant concentration would impact on the crystal structure and activation energies.

Table 3. Calculated activation energies of local Li hops (A and B).

Dopants	Activation Energy (eV)	
	A	**B**
Na	0.58	0.93
Fe	0.55	0.87
Al	0.54	0.86
Ga	0.56	0.84
Si	0.59	0.88

4. Conclusions

In conclusion, computational modelling based on classical potential was applied to analyze the behavior of the defects, diffusion properties and solution of dopants in $Li_2NiGe_3O_8$. The results of the calculations found that Li-Ni cation mixing is present at low concentrations in this material. Such cation mixing is expected to affect the properties of this material. A three-dimensional Li-ion migration pathway was constructed. The activation energy was 0.57 eV, in good agreement with the values reported in the experiment. The lower value implies higher Li-ion conductivity. The most favorable isovalent dopants on the Li, Ni and Ge sites are Na, Fe and Si, respectively. Both Li-interstitials and oxygen vacancies can be introduced by doping with Al or Ga on the Ge site. Additional Li-interstitials would enhance the capacity of $Li_2NiGe_3O_8$, and oxygen vacancies would facilitate Li-ion diffusion.

Supplementary Materials: The following are available online at https://www.mdpi.com/article/10.3390/cleantechnol4030038/s1. Figure S1: A schematic representation of the defect models; Table S1: Two-body Buckingham potentials used for the dopant oxides in $Li_2NiGe_3O_8$.

Author Contributions: Computation, N.K.; writing, R.S. and N.K.; analysis and editing, R.S., P.I. and N.K. All authors have read and agreed to the published version of the manuscript.

Funding: This research received no external funding.

Institutional Review Board Statement: Not applicable.

Informed Consent Statement: Not applicable.

Data Availability Statement: Not applicable.

Acknowledgments: The High Performance Computing Services at Imperial College London are acknowledged for providing computational facilities.

Conflicts of Interest: The authors declare no conflict of interest.

References

1. Armand, M.; Tarascon, J.M. Building better batteries. *Nature* **2008**, *451*, 652. [CrossRef] [PubMed]
2. Whittingham, M.S. Lithium Batteries and Cathode Materials. *Chem. Rev.* **2004**, *104*, 4271–4302. [CrossRef] [PubMed]
3. Padhi, A.K.; Nanjundaswamy, K.S.; Goodenough, J.B. Phospho-olivines as Positive Electrode Materials for Rechargeable Lithium Batteries. *J. Electrochem. Soc.* **1997**, *144*, 1188–1194. [CrossRef]
4. Islam, M.S.; Fisher, C.A.J. Lithium and sodium battery cathode materials: Computational insights into voltage, diffusion and nanostructural properties. *Chem. Soc. Rev.* **2014**, *43*, 185–204. [CrossRef] [PubMed]
5. Masquelier, C.; Croguennec, L. Polyanionic (Phosphates, Silicates, Sulphates) Frameworks as Electrode Materials for Rechargeable Li (or Na) Batteries. *Chem. Rev.* **2013**, *113*, 6552–6591. [CrossRef]
6. Soltani, M.; Beheshti, S.H. A comprehensive review of Lithium-ion capacitor: Development, modelling, thermal management and applications. *J. Energy Storage* **2021**, *34*, 102019. [CrossRef]
7. Delmas, C. Sodium and Sodium-Ion Batteries: 50 Years of Research. *Adv. Energy Mater.* **2018**, *8*, 1703137. [CrossRef]
8. Jeżowski, P.; Crosnier, O.; Brousse, T. Sodium borohydride (NaBH4) as a high-capacity material for next-generation sodium-ion capacitors. *Open Chem.* **2021**, *19*, 432–441. [CrossRef]
9. Hosaka, T.; Kubota, K.; Hameed, A.S.; Komaba, S. Research Development on K-Ion Batteries. *Chem. Rev.* **2020**, *120*, 6358–6466. [CrossRef]
10. Nik, R.M.; Ronald, I.S.; Anthony, R.W. Lithium-Ion conduction pathways in complex lithium spinels $Li_2MGe_3O_8$ (M = Ni or Zn). *Chem. Mater.* **2011**, *23*, 3556–3563.
11. Daniel, Z.C.M.; Abby, R.H.; Whiney, L.S.; Peter, J.B.; Rebecca, B.; Karen, E.J.; Nik, R.M. Evaluating lithium diffusion mechanisms in the complex spinel $Li|NiGe_3O_8$. *Phys. Chem. Chem. Phys.* **2019**, *21*, 23111–23118.
12. Bachman, J.C.; Muy, S.; Grimaud, A.; Chang, H.; Pour, N.; Lux, S.F.; Paschos, O.; Maglia, F.; Lupart, S.; Lamp, P.; et al. Inorganic Solid-State Electrolytes for Lithium Batteries: Mechanisms and Properties Governing Ion Conduction. *Chem. Rev.* **2016**, *116*, 140–162. [CrossRef]
13. Orera, A.; Campo, J. Influence of Li^+ and H^+ Distribution on the Crystal Structure of $Li_{7-x}H_xLa_3Zr_2O_{12}$ ($0 \leq x \leq 5$) Garnets. *Inorg. Chem.* **2016**, *55*, 1324–1332. [CrossRef]
14. Hofstetter, K.; Samson, A.J.; Narayanan, S.; Thangadurai, V. Present understanding of the stability of Li-stuffed garnets with moisture, carbon dioxide, and metallic lithium. *J. Power Sources* **2018**, *390*, 297–312. [CrossRef]
15. Bragg, W.H. The structure of the spinel group of crystals. *Philos. Mag.* **1915**, *30*, 305–315. [CrossRef]
16. Nishikawa, S. Structure of Some Crystals of Spinel Group. *Proc. Math. Phys. Soc. Tokyo* **1915**, *8*, 199–209.
17. Nakayama, M.; Jalem, R.; Kasuga, T. Electronic structure of spinel-type $LiNi_{1/2}Ge_{3/2}O_4$ and $LiNi_{1/2}Mn_{3/2}O_4$ as positive electrodes for rechargeable Li-ion batteries studied by first-principles density functional theory. *Solid State Ionics* **2014**, *262*, 74–76. [CrossRef]
18. Gale, J.D. GULP: A computer program for the symmetry-adapted simulation of solids. *J. Chem. Soc. Faraday Trans.* **1997**, *93*, 629–637. [CrossRef]
19. Kuganathan, N.; Islam, M.S. Li_2MnSiO_4 Lithium Battery Material: Atomic-Scale Study of Defects, Lithium Mobility, and Trivalent Dopants. *Chem. Mater.* **2009**, *21*, 5196–5202. [CrossRef]
20. Kuganathan, N.; Iyngaran, P.; Chroneos, A. Lithium diffusion in Li_5FeO_4. *Sci. Rep.* **2018**, *8*, 5832. [CrossRef]
21. Tealdi, C.; Saiful Islam, M.; Malavasi, L.; Flor, G. Defect and dopant properties of MgTa2O6. *J. Solid State Chem.* **2004**, *177*, 4359–4367. [CrossRef]
22. Gale, J.D.; Rohl, A.L. The General Utility Lattice Program (GULP). *Mol. Simul.* **2003**, *29*, 291–341. [CrossRef]
23. Mott, N.F.; Littleton, M.J. Conduction in polar crystals. I. Electrolytic conduction in solid salts. *Trans. Faraday Soc.* **1938**, *34*, 485–499. [CrossRef]
24. Kempaiah Devaraju, M.; Duc Truong, Q.; Hyodo, H.; Sasaki, Y.; Honma, I. Synthesis, characterization and observation of antisite defects in $LiNiPO_4$ nanomaterials. *Sci. Rep.* **2015**, *5*, 11041. [CrossRef]
25. Politaev, V.V.; Petrenko, A.A.; Nalbandyan, V.B.; Medvedev, B.S.; Shvetsova, E.S. Crystal structure, phase relations and electrochemical properties of monoclinic Li_2MnSiO_4. *J. Solid State Chem.* **2007**, *180*, 1045–1050. [CrossRef]
26. Kuganathan, N.; Chroneos, A. Defects, diffusion, dopants and encapsulation of Na in $NaZr_2(PO_4)_3$. *Materialia* **2021**, *16*, 101039. [CrossRef]
27. Kim, Y. Theoretical investigation of the cation antisite defect in layer-structured cathode materials for Li-ion batteries. *Phys. Chem. Chem. Phys.* **2019**, *21*, 24139–24146. [CrossRef]

28. Lin, Q.; Guan, W.; Zhou, J.; Meng, J.; Huang, W.; Chen, T.; Gao, Q.; Wei, X.; Zeng, Y.; Li, J.; et al. Ni–Li anti-site defect induced intragranular cracking in Ni-rich layer-structured cathode. *Nano Energy* **2020**, *76*, 105021. [CrossRef]
29. Kröger, F.A.; Vink, H.J. Relations between the Concentrations of Imperfections in Crystalline Solids. In *Solid State Physics*; Seitz, F., Turnbull, D., Eds.; Academic Press: New York, NY, USA, 1956; Volume 3, pp. 307–435.
30. Morando, C.; Cofrancesco, P.; Tealdi, C. Zn ion diffusion in spinel-type cathode materials for rechargeable batteries: The role of point defects. *Mater. Today Commun.* **2020**, *25*, 101478. [CrossRef]
31. Li, J.-J.; Dai, Y.; Zheng, J.-C. Strain engineering of ion migration in $LiCoO_2$. *Front. Phys.* **2021**, *17*, 13503. [CrossRef]
32. Azough, F.; Freer, R.; Wright, K.; Jackson, R. A computer simulation study of point defects in diopside and the self-diffusion of Mg and Ca by a vacancy mechanism. *Mineral. Mag.* **1998**, *62*, 599–606. [CrossRef]
33. Kilo, M.; Jackson, R.A.; Borchardt, G. Computer modelling of ion migration in zirconia. *Philos. Mag.* **2003**, *83*, 3309–3325. [CrossRef]